Heliyon 10 (2024) e30604

Contents lists available at ScienceDirect

Heliyon

journal homepage: www.cell.com/heliyon

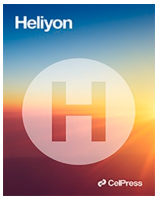

Research article

Efficient removal of oxytetracycline antibiotic from aqueous media using UV/g-C_3N_4/Fe_3O_4 photocatalytic process

Kourosh Mahmoudi [a,b], Mahdi Farzadkia [a,b], Roshanak Rezaei Kalantary [a,b], Hamid Reza Sobhi [c], Mojtaba Yeganeh [a,b], Ali Esrafili [a,b,*]

[a] Department of Environmental Health Engineering, School of Public Health, Iran University of Medical Sciences, Tehran, Iran
[b] Research Center for Environmental Health Technology, Iran University of Medical Sciences, Tehran, Iran
[c] Department of Chemistry, Payame Noor University, Tehran, Iran

ARTICLE INFO

Keywords:
Photocatalyst
Antibiotic
Oxytetracycline
UV/g-C_3N_4/Fe_3O_4

ABSTRACT

Residual pharmaceuticals in the environment are a class of emerging pollutants that endanger human health. Tetracycline's family, including oxytetracycline (OTC), are known as one of the most produced and consumed antibiotics worldwide. The g-C_3N_4/Fe_3O_4 nanocomposite with high level of catalytic efficiency features suitable performance in water/wastewater treatment. Therefore, in the present study, this nanocomposite was applied to remove the oxytetracycline from the aqueous environment. In this research study, g-C_3N_4/Fe_3O_4 nanocomposite (serving as catalyst) was initially synthesized by a simple hydrothermal method. The effect of key operating parameters such as initial solution pH, dose of catalyst, contact time and initial concentration of OTC in aqueous solutions was investigated under UV irradiation. In addition, COD and TOC tests, the kinetics and the effect of radical scavengers on the applied photocatalytic process were all evaluated. The maximum removal efficiency of OTC (99.8 %) was achieved under the following conditions: neutral solution pH 7; catalyst dose, 0.7 g/L; and an initial OTC concentration of 5 mg/L. The data showed that the kinetics of the reaction followed the first-order model with R^2 of 0.9755. The respective COD and TOC efficiency values for the applied photocatalytic process were determined to be 87 and 59 %, respectively. In addition, the lowest removal efficiency of OTC was observed in the presence of tert-butanol radical scavengers, and OH radicals played a main role. The UV/g-C_3N_4/Fe_3O_4 photocatalytic process proved to be highly efficient for the removal of OTC antibiotic and could be potentially applied for the removal of other pollutants from aqueous solutions.

1. Introduction

With no doubt, water remains the greatest asset for humans and other creatures to survive and continue life on the planet. Unfortunately, with increasing industrialization, rapid population growth, urbanization, and widespread agricultural activities, a sharp decline in quality of water resources is inevitable [1]. Water pollution poses a serious threat to human health, biodiversity and ecosystem stability, so that the quality of water resources has become a major concern for human beings [2].

* Corresponding author. Department of Environmental Health Engineering, School of Public Health, Iran University of Medical Sciences, Tehran, Iran.
E-mail address: a.esrafili@iums.ac.ir (A. Esrafili).

https://doi.org/10.1016/j.heliyon.2024.e30604
Received 17 February 2024; Received in revised form 29 April 2024; Accepted 30 April 2024
Available online 1 May 2024

Antibiotics have revolutionized medicine in many ways and their discovery is regarded as a corner stone in history. Nevertheless, the excessive use of these drugs has been associated with the rapid emergence of resistant strains [3]. The presence of antibiotics and their transformation products in the environment result in the creation of antibiotic-resistant bacteria and antibiotic-resistant genes [4]. The World Health Organization (WHO) has acknowledged antibiotic resistance as one of the three most important threats to public health in the 21st century [5].

Amongst the antibiotic pollutants contaminating water sources, tetracycline's family are known as the second most produced and consumed antibiotics worldwide [6]. Of this family, oxytetracycline (OTC) is widely used as a prescribed treatment and growth stimulant in veterinary medicine, poultry farming and aquaculture due to its medicinal properties [7]. This antibiotic features a complex four-ring structure bearing a number of ionizable functional groups (see Fig. 1) [8].

OTC enters the surface and underground water through household and hospital sewage, livestock and aquaculture centers. It also enters the human body through drinking, eating fruits and vegetables. Even at very low concentration, its appearance at a high frequency can cause bacteria-resistance and promote the production of antibiotic-resistant genes [8,9].

Dissemination of antibiotics in natural waters is mainly performed in the effluents of municipal sewage treatment plants (STPs) and pharmaceutical factories. Current wastewater treatment technologies are not sufficiently capable of removing antibiotics, so updated, efficient and low-cost technologies are high on demand [10]. Various methods have been applied to remove antibiotics from water and wastewater sources. In a study by Trovó AG et al., they applied photo-Fenton process to degrade Chloramphenicol [11] and also Arefi-Oskoui S et al. implemented the membrane process for the removal of Rifampicin [12]. In addition, Renyong Geng et al. utilized adsorption process for the removal of several antibiotics namely, chlorhexidine acetate, minocycline, and erythrocin [13]. In a simlary reported work, Hassan Mohamed NA applied the photocatalytic process for the degradation of some antibiotics namely, Ciprofloxacin, Ampicillin and Erythromycin [14]. Nevertheless, the main drawbacks associated with these above-mentioned methods are high level of energy consumption, high cost and low efficiency of mineralization [15]. Advanced oxidation processes (AOPs) featuring fast reaction rate and strong oxidation ability have received more attention than other methods used for the removal of antibiotics [16]. The photocatalytic process is categorized as one of the main advanced oxidation processes, in which a total mineralization of organic pollutants and their transformation into harmless and environmentally friendly products takes place. This process is on the basis of the reaction between organic pollutants and strong oxidation/reduction agents, which are generated by ultraviolet ray (UV) or visible light (Vis) on the surface of the catalysts [17].

In a heterogeneous photocatalytic process, a semiconductor material is employed with featuring a valence band (V_B) of low energy and a conduction band (C_B) of high energy. The distance between V_B and the C_B is recognized as the band gap of the semiconductor. It is clear cut that once the energy of radiation light is higher than the band gap of the semiconductor, the electrons in the V_B of the semiconductor are excited and transferred to the C_B and as a result the holes are created in the V_B. The generated electrons and holes (e^-/h^+, pairs) have strong oxidizing properties and are able to oxidize the potential pollutants adsorbed on the surface of semiconductor [18–21]. Recently, the graphite carbon nitride (g–C_3N_4)–based nanocomposites have been widely used for the photocatalytic degradation of various pollutants in water media. g-C_3N_4 is an organic polymer semiconductor featuring the wonderful properties such as compatibility with the environment, high chemical stability and low cost. Nevertheless, it is associated with several drawbacks including the possibility of rapid recombination of electron/hole pairs and difficult separation throughout the reaction in aqueous media. To remedy, a new method based on the doping of a semiconductor with metallic and non-metallic elements have been introduced. For instance, the coupling of Fe_3O_4 nanoparticles with g-C_3N_4 sheets seems to a viable choice of interest. The results of various research studies have demonstrated that the photocatalytic process using the combined g-C_3N_4/Fe_3O_4 nanocomposite is highly efficient for the degradation and removal of pollutants [22].

Therefore, in this study, g-C_3N_4/Fe_3O_4 nanocomposite was synthesized and characterized to remove the well-known antibiotic of OTC from aqueous solutions, and the efficiency of the photocatalytic process was evaluated through the optimization of influential factors involved. g-C_3N_4/Fe_3O_4 nanocomposite with high level of catalytic efficiency features suitable performance in water/

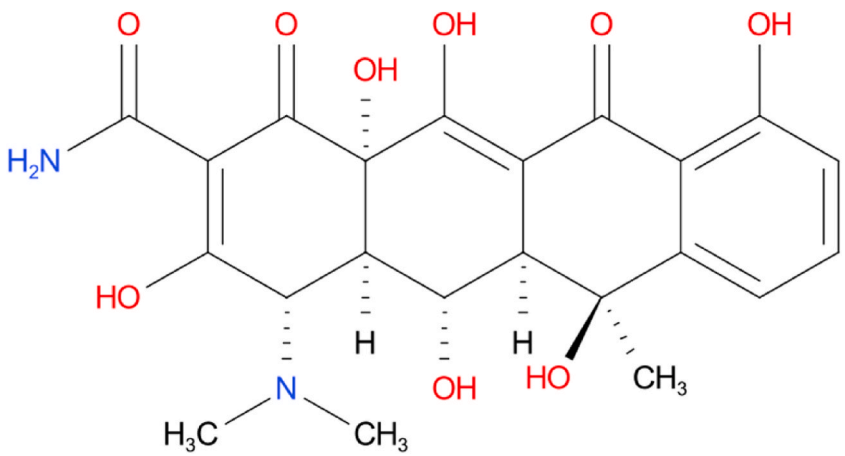

Fig. 1. Chemical structure of OTC.

wastewater treatment. Therefore, in the present study, this nanocomposite was applied as an efficient catalyst to remove OTC from the aqueous environment.

2. Methods and materials

2.1. Chemicals

The chemicals used in this study include OTC, melamine, ferric chloride hexahydrate, ferrous chloride tetrahydrate, ammonia, hydrochloric acid, sodium hydroxide, sulfuric acid, ethanol, and methanol, which were all purchased from Merck Company. In addition, distilled water was used throughout to prepare all aqueous solutions.

2.2. Preparation of nanocomposite

2.2.1. Synthesis of g-C_3N_4 powder

g-C_3N_4 was produced by direct calcination of melamine at 550 °C in a furnace. For this purpose, 5 g of melamine powder was poured in a ceramic crucible and placed in an oven at 550 °C for 4 h, after that the prepared g-C_3N_4 was cooled to room temperature.

2.2.2. Preparation of Fe_3O_4 nanoparticles

A modified co-precipitation method was implemented for the preparation of Fe_3O_4 nanoparticles [23]. Briefly, 4.72 g $FeCl_3{\cdot}6H_2O$ and 1.72 g $FeCl_2{\cdot}4H_2O$ were thoroughly mingled and dissolved in distilled water (100 ml) followed by the basification with NH_4OH (10 ml) The resulting mix was then vigorously mixed at 80 °C for 1 h. Finally, an external magnet was used to recover Fe_3O_4 nanoparticles which further were washed with pure water and ethanol, and eventually dried at 60 °C.

2.2.3. Preparation of g-C_3N_4/Fe_3O_4 nanocomposite

Initially, 0.07 g of g-C_3N_4 powder was weighed and added to 250 ml of 1:2 ethanol/water solution and the resulting suspension was placed in an ultrasound bath for 6 h. To the above suspension, 0.92 g of $FeCl_3{\cdot}6H_2O$ and 0.45 g of $FeCl_2{\cdot}4H_2O$ previously dissolved in 10 ml distilled water was added. The resulting mixture was stirred in at 80 °C for 30 min. Then, 10 ml of ammonia was added to the mixture while agitating for 30 min. The solution was then allowed to cool at ambient temperature. The obtained g-C_3N_4/Fe_3O_4 nanocomposite was separated from the solution by a magnet and washed several times with ethanol and water. Finally, the nanocomposite was dried at 60 °C for further studies [24].

2.2.4. Characteristics of g-C_3N_4/Fe_3O_4 nanocomposite

Following the synthesis of g-C_3N_4/Fe_3O_4 nanocomposite, its physiochemical properties were determined by a number of analytical instruments as follows: X-ray diffraction (XRD) analysis was applied to mainly determine the phases of the nanoparticles involved within 2ɵ of 10–80°. Field emission scanning electron microscopy (FE-SEM) was used to study the surface properties and morphology of the nanoparticles. Energy dispersive X-ray analysis (EDAX) was employed to identify the contribution of the elements within the structure of synthesized nanocomposite. In addition, Fourier transform infrared spectroscopy (FTIR) was used to identify the presence of main organic functional groups. UV–vis diffuse reflectance spectroscopy (DRS) spectra were obtained by a spectrophotometer. Finally, Vibrating-sample magnetometry (VSM) was used to verify the magnetic properties of the nanocomposite.

2.3. Photocatalytic degradation of OTC

The experiments with regard to photocatalytic degradation of OTC were carried out in a 2-L Pyrex reactor continuously agitated at ambient temperature. A UV-A lamp (15 W) was served as the radiation source. A mechanical stirrer was used to agitate the content of the reactor. A dilute solution of HCl/NaOH (0.1 M) was also used to adjust the pH of the aqueous sample solutions. It is noted that each experiment was repeated three times and the Excel software was used for the data analysis.

The variables studied in this research were optimized univarietly. During each experiment, the sampling of the solutions was done at specific time intervals (5–120 min) and the nanocomposite catalyst was separated off the solution using a magnet and the remaining concentration of OTC was determined by a HPLC (Cecil 4100, England), with a C18 column (250 nm × 4.6 mm × 5 μm) at 354 nm. The following equation was used to calculate the removal efficiency of OTC (Eq. (1)).

$$Removal\ (\%) = \frac{(C_0 - C_t)}{C_0} \times 100 \tag{1}$$

Where respective C_0 and C_t represent the initial and final concentration of OTC (mg/L).

The TOC values were measured by a total organic carbon analyzer (Multi N/C, TOC 3100 analyzer, Germany). The removal efficiency was calculated by the following equation (Eq. (2)):

$$TOC\ Removal\ (\%) = \frac{TOC_0 - TOC_t}{TOC_0} \times 100 \tag{2}$$

Where respective TOC_0 and TOC_t represent the initial and final TOC values.

3. Results and discussion

3.1. Characteristics of nanocomposite

In Fig. 2a, the XRD patterns of Fe_3O_4, g-C_3N_4 and g-C_3N_4/Fe_3O_4 nanoparticles are presented. g-C_3N_4 has two peaks at 13.5 and 27.4° corresponding to the tri-S-triazine unit with the file (JCPDS file number 87-15-26). The characteristic peaks within Fe_3O_4 structure are observed at 2θ = 30.2°, 35.6°, 43.3°, 53.7°, 57.3°, and 62.8°. These peaks are in line with the crystal planes of Fe_3O_4 corresponding to the JCPDS data: 19–0629 [25,26]. As shown, the XRD pattern of g-C_3N_4/Fe_3O_4 nanocomposite is composed of all the diffraction peaks belonging to g-C_3N_4 and Fe_3O_4, implying that g-C_3N_4/Fe_3O_4 was well synthesized.

In Fig. 2b, the FT-IR spectra of Fe_3O_4, g-C_3N_4 and g-C_3N_4/Fe_3O_4 nanoparticles are demonstrated. In the g-C_3N_4 structure, a sharp band at 808 cm^{-1} is related to the vibrational bending of triazine rings. The absorption band located within the region of 1200–1600 cm^{-1} is ascribed to the stretching mode of C–N/C═N belonging to the heterocyclic part of g-C_3N_4. The peaks at 1241, 1318, 1425, and 1635 cm^{-1} are assigned to the stretching mode of C–N aromatic rings. The respective broad adsorbed band at 3100-3400 cm^{-1} could be related to the vibration mode of N–H and O–H bonds belonging to the free amino groups and absorbed water molecules. In addition, the sharp band at 600-900 cm^{-1} is highly likely attributed to Fe–O tensile vibration.

FE-SEM images of g-C_3N_4 and g-C_3N_4/Fe_3O_4 nanoparticles are depicted in Fig. 3. Within the Figure is vividly seen that g-C_3N_4 is in sheet forms (Fig. 3(a and b)), while Fe_3O_4 particles are coated on g-C_3N_4 sheets (Fig. 3(c and d)).

EDAX patterns of g-C_3N_4, g-C_3N_4/Fe_3O_4 nanocomposite and the elemental mapping of g-C_3N_4/Fe_3O_4 are also shown in Fig. 1s (a, b and c). Accordingly, the presence of carbon and nitrogen elements in g-C_3N_4 structure and carbon, nitrogen, oxygen and iron elements within g-C_3N_4/Fe_3O_4 nanocomposite are visibly seen. The elemental mappings of g-C_3N_4/Fe_3O_4 nanocomposite (Fig. 1s(c)) reaffirmed the uniform arrangement of all elements involved, including C, N, O and Fe.

The DRS experimental test was employed to determine the properties with respect to the optics of the nanocomposite. Fig. 2S(a) shows the UV–vis DRS spectra of g-C_3N_4, Fe_3O_4 and g-C_3N_4/Fe_3O_4 nanocomposites. Accordingly, the utmost absorption band was obtained within the UV region (300–350 nm), which corresponds to the excitation band gap of the applied catalyst.

Meanwhile, the Kubelka-Munk function was used to estimate the band gap energy of the nanocomposites (Fig. 2S(b)) [27]. The respective band gap energies for g-C_3N_4, Fe_3O_4 and g-C_3N_4/Fe_3O_4 nanocomposites were measured to be 2.7, 2.23 and 1.7 eV. It can be deduced that the band gap of g-C_3N_4 declined once it was integrated with Fe_3O_4 nanoparticles. This leads to the promotion of the photocatalytic efficiency with regard to the g-C_3N_4/Fe_3O_4 nanocomposite.

VSM analysis was performed to determine the magnetic properties of g-C_3N_4/Fe_3O_4 nanocomposite. As it is clear in Fig. 4, due to the presence of magnetic particles of Fe_3O_4 within the nanocomposite structure, a favorable magnetic property is associated with the catalyst.

In a further related identification analysis, the pHzpc of the nanocomposite was determined to be 7.8 (see Fig. 3s). It is clear cut that at this pH, the surface charge of the catalyst is zero and the catalyst remains neutral.

3.2. Optimization of influential parameters

3.2.1. Effect of pH

The effect of variations in the initial pH of the solution within the range of 3–11 containing the antibiotic OTC on the efficiency of the photocatalytic process is illustrated (see Fig. 5). As can be seen, the maximum removal rate of OTC was observed at pH = 7 (89.3 %). Therefore, neutral pH (i.e., 7) was chosen as the optimal pH for further experiments.

Meanwhile, pH_{zpc} of the catalyst as an important factor for finding out the OTC removal mechanism involved was determined to be

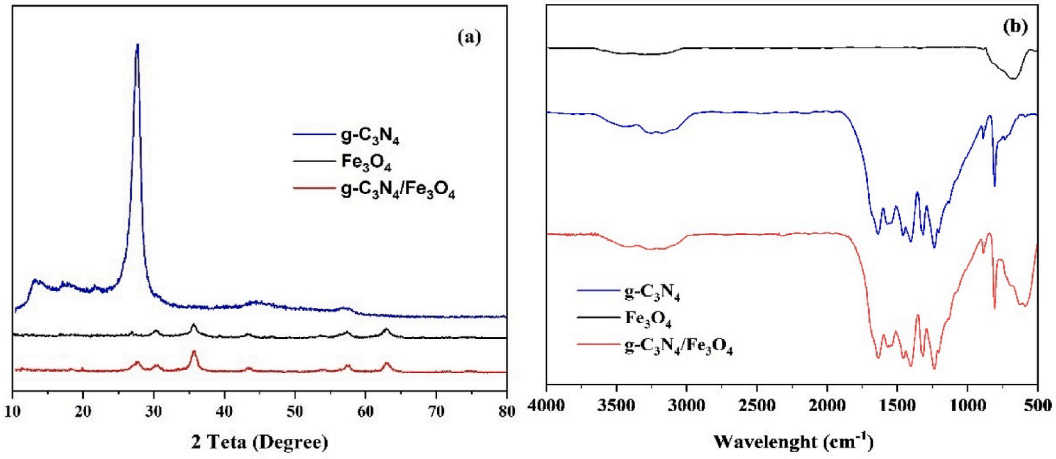

Fig. 2. XRD patterns of Fe_3O_4, g-C_3N_4 and g-C_3N_4/Fe_3O_4 (a), FT-IR images of Fe_3O_4, g-C_3N_4 and g-C_3N_4/Fe_3O_4 (b).

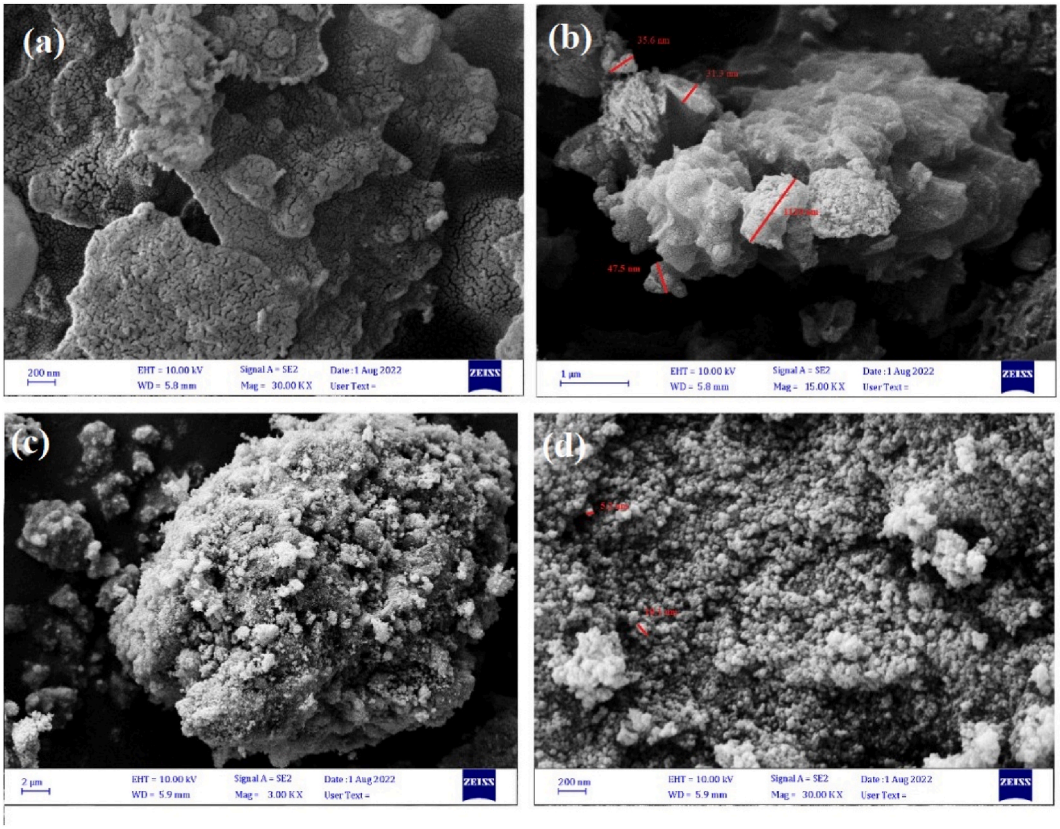

Fig. 3. FE-SEM images of g-C_3N_4 (a and b) and g-C_3N_4/Fe_3O_4 (c and d).

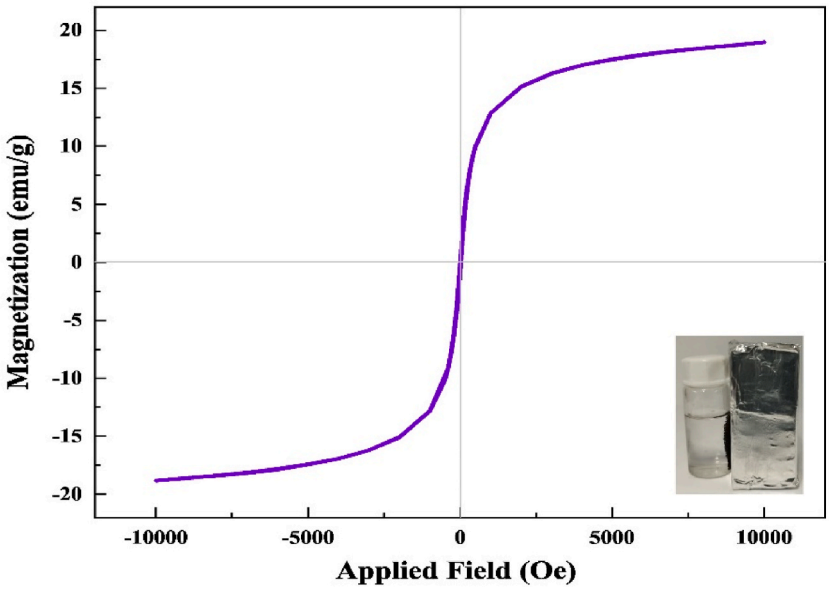

Fig. 4. VSM analysis of g-C_3N_4/Fe_3O_4 nanocomposite.

7.8. At pH $\leq$ pH_{zpc} values, the catalyst surface is positively charged; whilst at pH $\geq$ pH_{zpc}, it is negatively charged. Therefore, it is expected that the efficiency of the photocatalytic process alters under different pH values. In addition, varying the pH of the reaction medium definitely results in the changes of the surface charge of the catalyst [28,29]. OTC antibiotic has been reported to have two

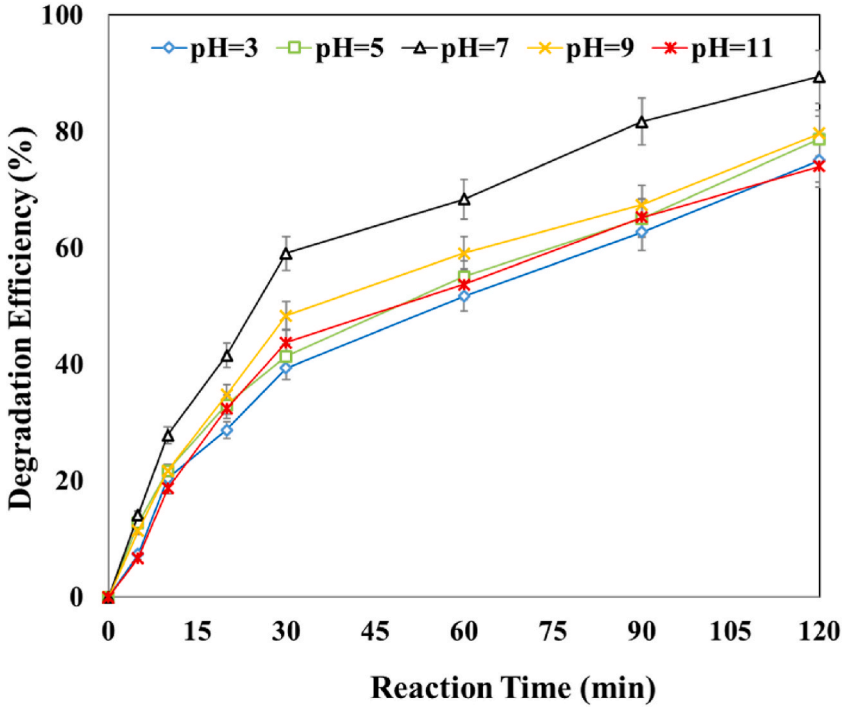

Fig. 5. Effect of variation of pH of solution on the efficiency of the photocatalytic process (catalyst dose = 0.5 g/L, initial OTC concentration = 30 mg/L).

pK_as ($pK_a1 = 3.18$ and $pK_a2 = 8.29$) [30]. Thus, once pH < 3.18, the cationic form of OTC is dominant (OTC^+), whilst at pH > 8.29 the anionic form (OTC^-) is a major species in the aqueous solution [31]. Given the pH_{zpc} of the catalyst used (i.e., 7.8) and the optimal solution pH earlier obtained (i.e., 7), it is thought that the molecular form of OTC is adsorbed on the surface of the catalyst. This adsorption is likely related to the strong electrostatic interactions between the catalyst surface and the functional groups of OTC [32, 33]. In a study by Xu et al. they demonstrated that the efficiency of the photocatalytic process was enhanced in the presence of the

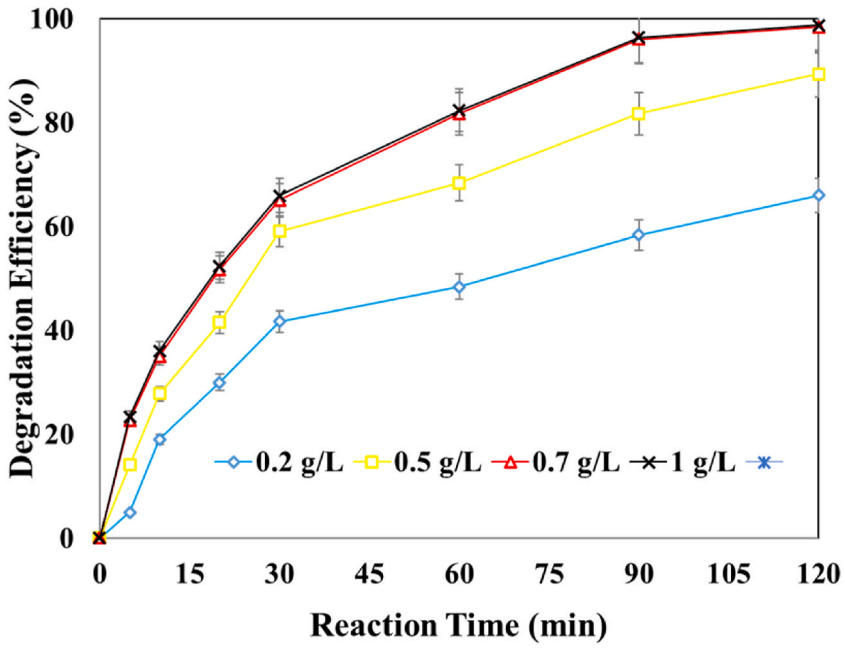

Fig. 6. Effect of catalyst dose on the efficiency of the photocatalytic process (pH = 7, and initial antibiotic concentration = 30 mg/L).

magnetic nanocomposite g-C_3N_4/Fe_3O_4 for the removal of catechol. In this study, the efficiency of the process was reported to be highest at pH 7 than other pH values [34]. In another related study by Chi et al. they also reported the maximum photocatalytic removal of arsenate was obtained at about neutral pH in the presence of the g-C_3N_4/Fe_3O_4 catalyst [35].

3.2.2. Effect of catalyst dosage

In Fig. 6, the effect of the catalyst dosage ranging from 0.2 to 1.0 g/L on the efficiency of the photocatalytic process is shown. As illustrated, the efficiency of the process enhanced (98 %) by increasing the dose of the catalyst (up to 0.7 g/L) and thereafter levelled out. Therefore, the value of 0.7 g/L for the optimal catalyst dose was chosen.

An improvement in the efficiency of the process which followed the rise in the dose of the catalyst could be attributed to an increase in the number of active sites on the catalyst surface. The tiny drop in the efficiency of the process (observed between the corresponding values of 0.7 and 1.0 g/L) could be related to the fact that high amounts of catalyst in the solution prevents the effective penetration of UV into the reactor. In addition, high amounts of catalyst can lead to an increase in the production of hydroxyl radicals resulting in a decrease in the efficiency [36]. In a study conducted by Zhang et al. the optimal dose of g-C_3N_4/Fe_3O_4 catalyst was determined as 0.4 g/L [37]. Also, in a further related study by Ghodsi et al. the optimal amount of catalyst in diazinon removal was determined to be 0.5 g/L [38].

3.2.3. Effect of initial concentration of OTC antibiotic

The effect of changes in the initial concentration of the antibiotic OTC (within the range 5–50 mg/L) on the efficiency of the photocatalytic process is depicted in Fig. 7. According to the results obtained, the efficiency of the photocatalytic process dropped as the initial concentration of OTC increased. This finding is explained by the fact that by increasing OTC concentration and consequent further UV absorption, a decline in the rate of production of radical species, which are responsible for the degradation of OTC, takes place leading to a reduction in the removal efficiency of the photocatalytic process [39]. Tang et al. investigated the efficiency of the photocatalytic process in the removal of methylene blue and rhodamine B dyes and found out that with an increase in the concentration of the both dyes, the efficiency of the process decreased [40]. In an almost similarly related report by Berkani et al. the efficiency of the photocatalytic process in the removal of penicillin G decreased as the concentration of the pollutant increased and the best removal efficiency was obtained at the concentration of 5 mg/L [41].

3.3. Radical scavenger studies

In this experiment, the respective three well-known radical scavengers namely, tert-butanol (TBA), benzoquinone (BQ) and potassium iodide (KI) were used to investigate the influence of hydroxyl (OH°), superoxide ($O_2^{\circ-}$) and hole (h^+) on the efficiency of the photocatalytic process under the optimal conditions established earlier. As shown in Fig. 8, the presence of all three radical scavengers led to the reduction of OTC removal efficiency through the consumption of hydroxyl radical (OH°), superoxide radical ($O_2^{\circ-}$) and hole (h^+). It is reported that the radical scavenging agents have led to a decline in the efficiency of oxidation/reduction reactions in the

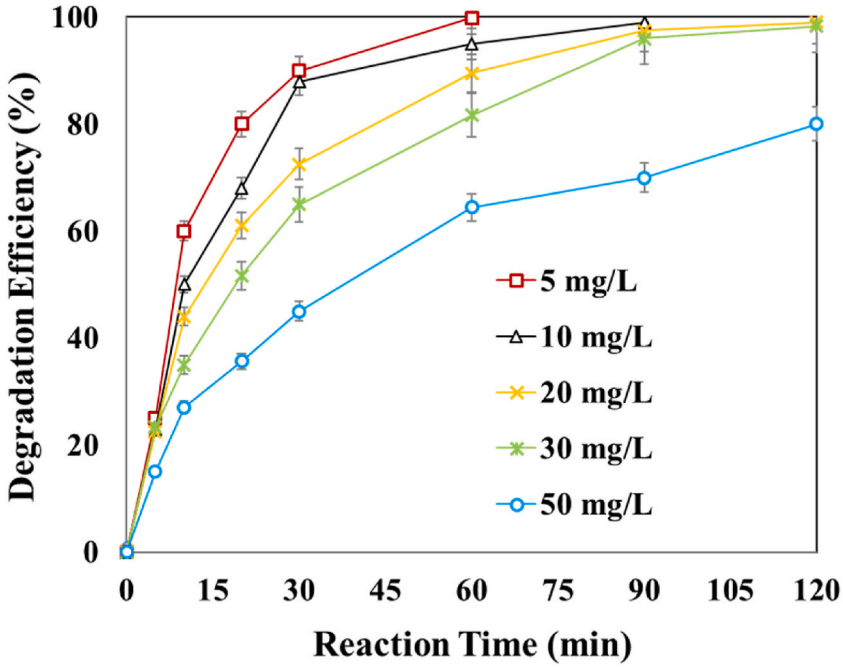

Fig. 7. Effect of initial concentration of OTC on the efficiency of the photocatalytic process (pH = 7, catalyst dose = 0.7 g/L).

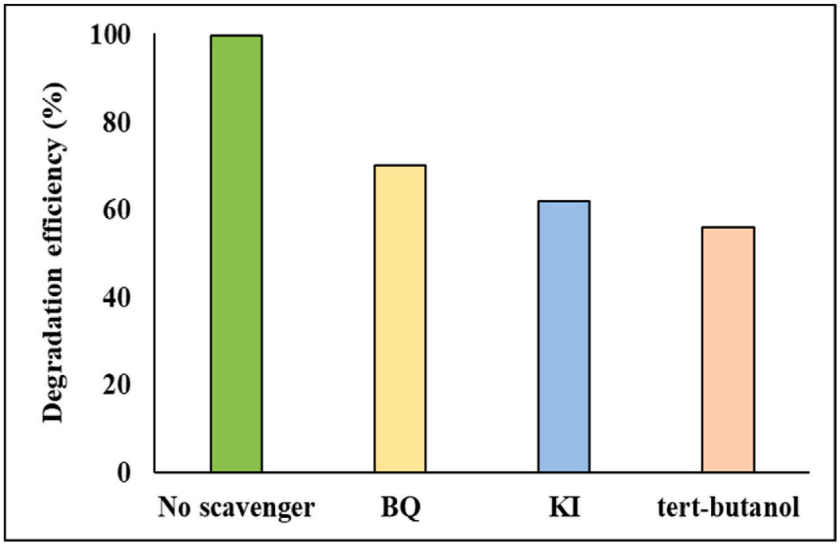

Fig. 8. Effect of radical scavengers on the efficiency of the photocatalytic process (pH = 7, catalyst dose = 0.7 g/L, OTC concentration = 5 mg/L, scavenger concentration = 0.5 mmol/L and time = 60 min).

photocatalytic process [42]. Hao et al. investigated the presence of scavengers in the removal of RhB in the photocatalytic process and revealed that hydroxyl radical, superoxide radical and h^+ were the main active species in the decomposition of RhB [43].

3.4. Reusability and stability of g-C_3N_4/Fe_3O_4

In a different experiment, the stability and reusability of g-C_3N_4/Fe_3O_4 catalyst was tested. Under the optimal conditions, following four consecutive cycles of use, the efficiency of the photocatalytic process did not almost alter and just a tiny drop (<5 %) was observed (see Fig. 4s). This implies that the applied catalyst in this study features great stability and reusability and can be reused at least for four times with almost no drop in its efficiency. In a study conducted by Sarkar et al. the applied catalyst was used over four consecutive cycles and the removal efficiency of the process remained almost unchanged [44]. In a similarly related report by Gupta et al. the same results were obtained as well [45].

3.5. Kinetics of photocatalytic process

The mathematical relationships and the corresponding reaction rate coefficients (R^2) based on the zero-order, first-order, pseudo-first-order, and second-order kinetic models are tabulated in Table 1.

The results obtained revealed that the kinetics of the process follows the first-order model. In a first-order kinetic model, the rate of reaction is proportional to the concentration of reactant (pollutant). The highest coefficient calculated ($R^2 = 0.9755$) implies that the active species are sufficiently produced during the removal process [39]. In a study by Wang et al. they investigated the efficiency of the photocatalytic process in the degradation of fluoroquinolones' antibiotics using g-C_3N_4 nanoparticles and found out that the kinetics followed the first-order model [46]. Furthermore, in a study by Liu et al. they also reported that the kinetics involved in the photocatalytic process using g-C_3N_4 and ZnO, best fitted to the first-order model [47].

3.6. Determination of COD and TOC values

The efficiency of the applied photocatalytic process with regard to the reduction of COD and TOC values under the optimal conditions is illustrated in Fig. 5s. Based on the results, the applied photocatalytic process can reduce COD and TOC values to a great extent.

As shown, under the optimal conditions, the COD and TOC efficiency values for the photocatalytic process with regard to the

Table 1
Kinetic data of the photocatalytic process (pH = 7, catalyst dose = 0.7 g/L, and OTC concentration = 5 mg/L).

Kinetic model							
Zero-order		First-order		Pseudo-First-order		Second-order	
k	R^2	k	R^2	k	R^2	k	R^2
0.0748	0.7031	0.0372	0.9755	0.039	0.5027	0.0047	0.9393

removal of OTC antibiotic were reduced and determined to be 87 and 59 %, respectively. In a study by Ata et al. the respective efficiency values of COD and TOC were reported to be within the range of 62–79 % and 62–86 % using the NFC-doped catalyst [48]. Furthermore, in a study by Kordestani et al. they reported that only 59.8 % of the initial COD and 48.7 % of the initial TOC were reduced in ceftriaxone removal case [49].

3.7. Contribution of involving components to OTC degradation

A number of control tests were performed to find out the contribution of each individual component engaged in the photodegradation process. In this regard, the degree of contribution concerning each individual component involved in the OTC degradation was determined. For this aim, five involving components, namely UV, UV/g-C_3N_4, UV/Fe_3O_4, UV/g-C_3N_4/Fe_3O_4 and g-C_3N_4/Fe_3O_4 were applied separately under the established optimum conditions and 60 min of contact time. As depicted in Fig. 9, the respective values of the degradation efficiency of OTC for each component were as follows: g-C_3N_4/Fe_3O_4 (11.8 %) and UV (20.1 %), UV/g-C_3N_4 (38.2 %), UV/Fe_3O_4 (29.5 %) and UV/g-C_3N_4/Fe_3O_4 (99.8 %). These results are indicative of a synergetic effect, which stems from the integration of UV light irradiation and the nanocomposite. It is concluded that the combined system (UV/g-C_3N_4/Fe_3O_4) definitely facilitates the degradation process [37].

3.8. Real environmental samples

The efficiency and applicability of the applied photocatalytic process in two real environmental samples (tap water and treated wastewater) were also assessed under the optimal conditions earlier established. The results showed that the tiny drop in the efficiency of the photocatalytic process was observed once the tap water was tested. This can be due to the presence of various cations and anions in the tap water, which may serve as radical or interfering scavengers. In the case of the wastewater the corresponding drop in the efficiency of the photocatalytic process was more appreciable (see Fig. 10). According to the reports published, the presence of some anions and cations in water sources competing with the target pollutant(s) lead to the consumption of active radicals and thereby reduces the efficiency of the process [50]. In a study by Yazdanbakhsh et al. the efficiency of the photocatalytic process in the removal of the antibiotic sulfamethoxazole in wastewater samples was reduced from 100 to 92 % [39]. It should be also noted that the presence of organic compounds such as humic acid may reduce the efficiency of the photocatalytic process. In further related studies by Xie et al. [51], almost similar report on the reduction of the efficiency of the photocatalytic process in wastewater samples were released.

3.9. Photocatalytic mechanism

The possible mechanism with regard to OTC photo degradation process using the catalyst (g-C_3N_4/Fe_3O_4) under UV-irradiation is depicted in Scheme 1. The values (band gap energy levels) of the valence band (VB) and conduction band (CB) of g-C_3N_4 and Fe_3O_4 nanoparticles were calculated using the following empirical formula (Eq. (3) and (4)).

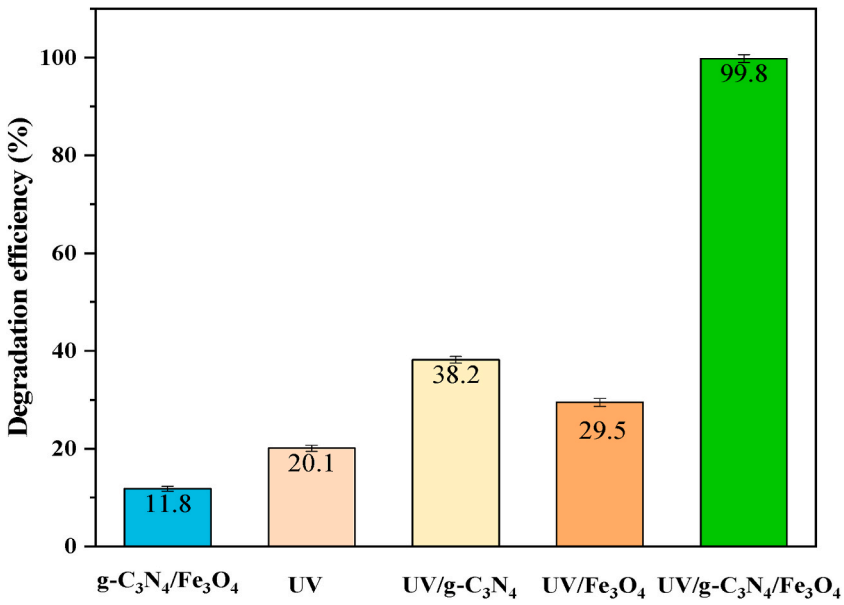

Fig. 9. Contribution of each component engaged in the degradation of efficiency of OTC under the optimum conditions (pH = 7, catalyst dose = 0.7 g/L, OTC concentration = 5 mg/L and time = 60 min).

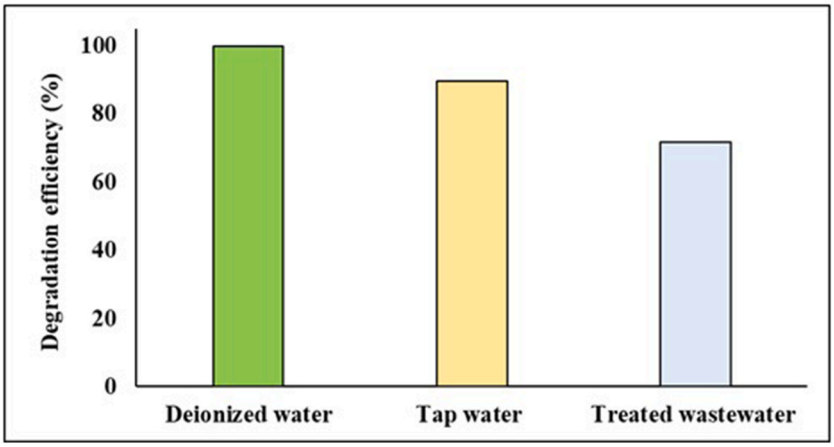

Fig. 10. Efficiency of the photocatalytic process in OTC removal in real environmental samples (pH = 7, catalyst dose = 0.7 g/L, OTC concentration = 5 mg/L and time = 60 min).

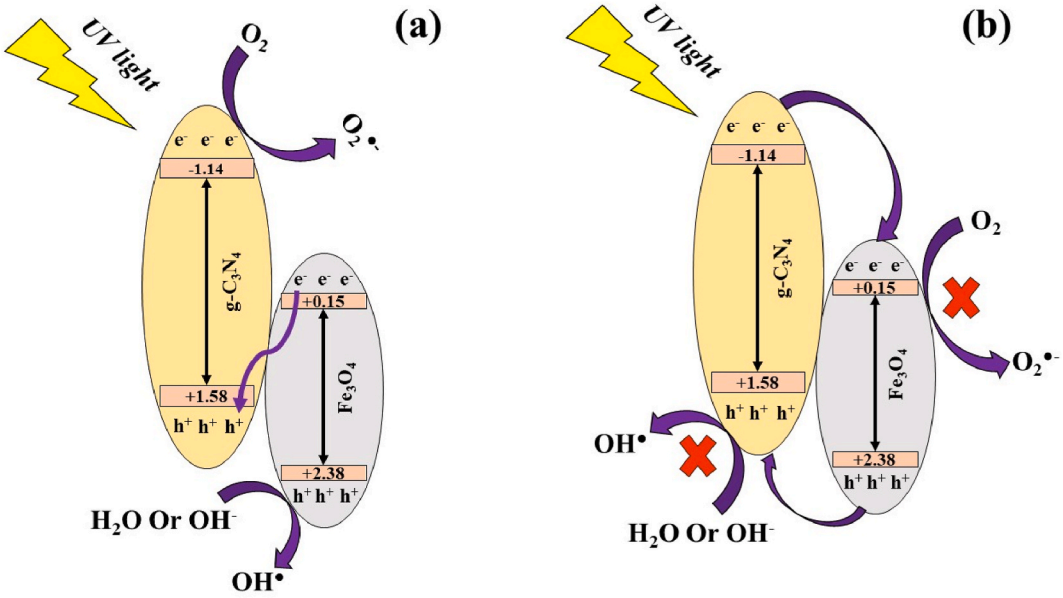

Scheme 1. Illustration of the photocatalytic mechanism using Fe_3O_4/g-C_3N_4 catalyst for simultaneous OTC degradation: S-scheme heterojunction (a) and type-II heterojunction (b).

$$E_{VB} = \chi - E_e + 1/2E_g \tag{3}$$

$$E_{CB} = E_{VB} - E_g \tag{4}$$

Eg represents the band gap values; X denotes the Mulliken's absolute electronegativity (X-g-C_3N_4 = 4.72 eV and X–Fe_3O_4 = 5.73 eV); Ee outlines the energy of free electrons (4.5 eV). The CB and VB values for g-C_3N_4 were determined to be −1.14 eV and +1.58 eV and the corresponding values for Fe_3O_4 were +0.15 eV and +2.38 eV, respectively.

Scheme 1 (a) illustrates the S-scheme heterojunction-based mechanism through the charge transfer within Fe_3O_4/g-C_3N_4 catalyst under UV-light irradiation. As the applied catalyst is exposed to UV-light irradiation, the electrons are excited resulting in the production of electron-hole pairs (Eq. (5)).

The electrons in the CB of Fe_3O_4 could be transferred to the VB of g-C_3N_4, where the reintegration with the remaining holes takes place. Since the CB value of g-C_3N_4 is more negative than the corresponding potential value of $O_2/O_2^{\circ-}$ (−0.33 eV vs. NHE), its CB electrons could be transferred to the O_2 molecules and produce $O_2^{\circ-}$ particles (Eq. (6)). In addition, the holes in the VB of Fe_3O_4 could oxidize H_2O/OH^- and generate HO° Eqs. (7)–(9)), due to be of more positive energy level than standard potentials of HO°/OH^- (1.99 eV vs. NHE) and HO°/H_2O (2.34 eV vs. NHE), In turn, the $O_2^{\circ-}$ and HO° species could degrade OTC under UV light irradiation (Eq.

(10)) [52–55].

Provided that the charge transfer involving the electron-hole pairs generated by UV light follows the pattern observed in conventional heterojunction systems (Scheme 1(b)), the electrons are pushed away from the CB of g-C_3N_4 to the CB of Fe_3O_4, while the holes located onto the VB of Fe_3O_4 are transferred to the VB of g-C_3N_4. Due to the lower potential VB of g-C_3N_4 than that of HO°/OH^- (1.99 eV vs. NHE) and HO°/H_2O (2.34 eV vs. NHE), the oxidation of OH^-/H_2O for the generation of HO° seems unlikely. Therefore, the electrons in the CB of Fe_3O_4 cannot react with O_2 to produce $O_2^{\circ -}$ radicals, because the CB potential value of Fe_3O_4 is not more negative than potential of the $O_2/O_2^{\circ -}$ (−0.33 eV vs. NHE) [55–57].

Considering all mentioned points and Scheme 1 (a and b), the proposed S-scheme heterojunction-based mechanism seems to be suitable to explain and elucidate the degradation of OTC using g-C_3N_4/Fe_3O_4 catalyst under UV irradiation.

$$\text{g-}C_3N_4/\ Fe_3O_4 + hv \rightarrow e^- + h^+ \quad (5)$$

$$O_2 + e^- \rightarrow O_2^{-\circ} \quad (6)$$

$$OH^- + h^+ \rightarrow HO^{\cdot} \quad (7)$$

$$2H_2O + h^+ \rightarrow H_2O_2 + 2H^+ \quad (8)$$

$$H_2O_2 + e^- \rightarrow OH^- + OH^\circ \quad (9)$$

$$\text{OTC} + \text{Reactive species } (HO^\circ, O_2^{\circ -}) \rightarrow \text{degradation products} + CO_2 + H_2O \quad (10)$$

3.10. A comparative-based study

Herein, a number of previously reported studies on the photocatalytic degradation of OTC published elsewhere were summarized in Table 2 [30,58–62]. As can be seen, the efficiency and merits of this research study concerning the decomposition and removal of OTC are fairly comparable with the other reports.

4. Conclusion

Herein, g-C_3N_4/Fe_3O_4 nanocomposite was initially prepared by a simple hydrothermal method and applied as the efficient catalyst for the efficient removal of a well-known antibiotic namely, OTC from the aqueous environmental samples under UV irradiation. Following that, the effect of major operating parameters affecting the photocatalytic process was individually optimized and then the optimal conditions for the removal of OTC in aqueous media were established. Moreover, the effect of radical scavengers on the applied photocatalytic process was evaluated in detail. The maximum removal efficiency of 99.8 % was achieved for OTC under the optimal conditions set. The utmost degradation efficiency of 99.8 % was achieved for OTC under neutral pH 7; catalyst dose, 0.7 g/L; and an initial OTC concentration of 5 mg/L. In addition, the kinetic results well fitted to the first-order model with R^2 of 0.9755. The respective COD and TOC efficiency values for the applied photocatalytic process were obtained to be 87 and 59 %, respectively. Additionally, the lowest degradation efficiency for OTC was observed in the presence of tert-butanol radical scavengers, and the OH radicals played a key role in that regard. Finally, the combined UV/g-C_3N_4/Fe_3O_4 photocatalytic process proved to be highly efficient for the removal of OTC antibiotic in several real water sources and could be potentially applied for the removal of other pollutants from aqueous solutions.

Data availability

The datasets generated and analyzed during the current study were available from the corresponding author on reasonable request.

Table 2
Comparative study on the photocatalytic degradation of OTC.

Photocatalyst	Light Source	C (mg/L)	Time (min)	R (%)	References
CoFe@NSC	visible light	50	150	90	[58]
TiO_2/5A zeolite	UV	50	150	100	[30]
g-C_3N_4/$LaFeO_3$ (2 %)	visible light	40	120	90	[59]
B_4NbO_8Cl/g-C_3N_4	visible light	20	60	87	[60]
ZnO/ZrO_2	UV	10	120	69	[61]
Br (15 %)/g-C_3N_4	visible light	10	120	75	[62]
g-C_3N_4/Fe_3O_4	UV	5	60	99.8	This work

CRediT authorship contribution statement

Kourosh Mahmoudi: Methodology, Investigation. **Mahdi Farzadkia:** Methodology, Investigation. **Roshanak Rezaei Kalantary:** Validation, Methodology. **Hamid Reza Sobhi:** Conceptualization. **Mojtaba Yeganeh:** Methodology. **Ali Esrafili:** Validation, Supervision.

Declaration of competing interest

The authors declare that they have no known competing financial interests or personal relationships that could have appeared to influence the work reported in this paper.

Acknowledgment

The authors would like to gratefully appreciate the Iran University of Medical Sciences for the provision of financial supports (Grant No. 1400-1-2-19943).

Appendix A. Supplementary data

Supplementary data to this article can be found online at https://doi.org/10.1016/j.heliyon.2024.e30604.

References

[1] K. Jain, A.S. Patel, V.P. Pardhi, S.J.S. Flora, Nanotechnology in wastewater management: a new paradigm towards wastewater treatment, Molecules 26 (2021) 1797.
[2] V.A. Tzanakakis, N.V. Paranychianakis, A.N. Angelakis, Water Supply and Water Scarcity, MDPI, 2020, p. 2347.
[3] J. Davies, D. Davies, Origins and evolution of antibiotic resistance, Microbiol. Mol. Biol. Rev. 74 (2010) 417–433.
[4] A.S. Oberoi, Y. Jia, H. Zhang, S.K. Khanal, H. Lu, Insights into the fate and removal of antibiotics in engineered biological treatment systems: a critical review, Environ. Sci. Technol. 53 (2019) 7234–7264.
[5] J. Munita, C. Arias, Mechanisms of antibiotic resistance. Virulence mechanisms of bacterial pathogens, Microbiol. Spectr. 2016 (2016) 481–511.
[6] R. Daghrir, P. Drogui, Tetracycline antibiotics in the environment: a review, Environ. Chem. Lett. 11 (2013) 209–227.
[7] B.L. Rivas, P. Oñate, D.A. Palacio, Removal of oxytetracycline by polymers. an overview, J. Chil. Chem. Soc. 65 (2020) 4943–4947.
[8] Z.-j. Li, W.-n. Qi, F. Yao, Y.-w. Liu, S. Ebrahim, L. Jian, Degradation mechanisms of oxytetracycline in the environment, J. Integr. Agric. 18 (2019) 1953–1960.
[9] C. Zhao, H. Deng, Y. Li, Z. Liu, Photodegradation of oxytetracycline in aqueous by 5A and 13X loaded with TiO_2 under UV irradiation, J. Hazard Mater. 176 (2010) 884–892.
[10] M.B. Ahmed, J.L. Zhou, H.H. Ngo, W. Guo, Adsorptive removal of antibiotics from water and wastewater: progress and challenges, Sci. Total Environ. 532 (2015) 112–126.
[11] A.G. Trovó, V.A. de Paiva, A.E. Machado, C.A. de Oliveira, R.O.J.S.E. Santos, Degradation of the antibiotic chloramphenicol by photo-Fenton process at lab-scale and solar pilot plant: kinetic, toxicity and inactivation assessment 97 (2013) 596–604.
[12] S. Arefi-Oskoui, A. Khataee, S.J. Behrouz, V. Vatanpour, S.H. Gharamaleki, Y. Orooji, M.J.S. Safarpour, P. Technology, Development of MoS_2/O-MWCNTs/PES Blended Membrane for Efficient Removal of Dyes, Antibiotic, and Protein, vol. 280, 2022 119822.
[13] R. Geng, J. Wang, Z. Zhang, Q. Dong, F. Wu, S. Chen, T. Su, X.J.C.E.J. Qi, Adsorption of Antibiotics by Polydopamine-Modified Salecan Hydrogel: Performance, Kinetics and Mechanism Studies, vol. 454, 2023 140446.
[14] N.A. Hassan Mohamed, R.N. Shamma, S. Elagroudy, A.J.R. Adewuyi, Visible light-driven photocatalytic degradation of ciprofloxacin, ampicillin and erythromycin by zinc ferrite immobilized on chitosan 11 (2022) 81.
[15] M. Yeganeh, H.R. Sobhi, A. Esrafili, Efficient photocatalytic degradation of metronidazole from aqueous solutions using Co/g-C_3N_4/Fe_3O_4 nanocomposite under visible light irradiation, Environ. Sci. Pollut. Control Ser. 29 (2022) 25486–25495.
[16] M.Z. Akbari, Y. Xu, Z. Lu, L. Peng, Review of antibiotics treatment by advance oxidation processes, Environmental Advances 5 (2021) 100111.
[17] D. Zhu, Q. Zhou, Action and mechanism of semiconductor photocatalysis on degradation of organic pollutants in water treatment: a review, Environ. Nanotechnol. Monit. Manag. 12 (2019) 100255.
[18] F. Zhang, X. Wang, H. Liu, C. Liu, Y. Wan, Y. Long, Z. Cai, Recent advances and applications of semiconductor photocatalytic technology, Appl. Sci. 9 (2019) 2489.
[19] J. Hua, Z. Wang, J. Zhang, K. Dai, C. Shao, K. Fan, A hierarchical Bi-MOF-derived BiOBr/Mn0. 2Cd0. 8S S-scheme for visible-light-driven photocatalytic CO_2 reduction, J. Mater. Sci. Technol. 156 (2023) 64–71.
[20] H. Yang, K. Dai, J. Zhang, G. Dawson, Inorganic-organic hybrid photocatalysts: syntheses, mechanisms, and applications, Chin. J. Catal. 43 (2022) 2111–2140.
[21] H. He, Z. Wang, K. Dai, S. Li, J. Zhang, LSPR-enhanced carbon-coated In_2O_3/$W_{18}O_{49}$ S-scheme heterojunction for efficient CO_2 photoreduction, Chin. J. Catal. 48 (2023) 267–278.
[22] S. Ghodsi, A. Esrafili, H.R. Sobhi, R. Rezaei Kalantary, M. Gholami, Synthesis and application of g-C_3N_4/Fe_3O_4/Ag nanocomposite for the efficient photocatalytic inactivation of Escherichia coli and Bacillus subtilis bacteria in aqueous solutions, Amb. Express 11 (2021) 1–12.
[23] H.R. Sobhi, M. Ghambarian, M. Behbahani, A. Esrafili, Application of dispersive solid phase extraction based on a surfactant-coated titanium-based nanomagnetic sorbent for preconcentration of bisphenol A in water samples, J. Chromatogr. A 1518 (2017) 25–33.
[24] M. Wang, S. Cui, X. Yang, W. Bi, Synthesis of g-C_3N_4/Fe_3O_4 nanocomposites and application as a new sorbent for solid phase extraction of polycyclic aromatic hydrocarbons in water samples, Talanta 132 (2015) 922–928.
[25] R. Yang, Q. Peng, B. Yu, Y. Shen, H. Cong, Yolk-shell Fe_3O_4@ MOF-5 nanocomposites as a heterogeneous Fenton-like catalyst for organic dye removal, Separ. Purif. Technol. 267 (2021) 118620.
[26] H. Alijani, A. Noori, N. Faridi, S.Z. Bathaie, M.F. Mousavi, Aptamer-functionalized Fe_3O_4@MOF nanocarrier for targeted drug delivery and fluorescence imaging of the triple-negative MDA-MB-231 breast cancer cells, J. Solid State Chem. 292 (2020) 121680.
[27] A.A. Isari, F. Hayati, B. Kakavandi, M. Rostami, M. Motevassel, E. Dehghanifard, N, Cu co-doped TiO_2@functionalized SWCNT photocatalyst coupled with ultrasound and visible-light: an effective sono-photocatalysis process for pharmaceutical wastewaters treatment, Chem. Eng. J. 392 (2020) 123685.
[28] Y. Liu, X. He, X. Duan, Y. Fu, D.D. Dionysiou, Photochemical degradation of oxytetracycline: influence of pH and role of carbonate radical, Chem. Eng. J. 276 (2015) 113–121.

[29] L. Liu, Z. Wang, J. Zhang, O. Ruzimuradov, K. Dai, J.J.A.M. Low, Tunable interfacial charge transfer in a 2D–2D composite for efficient visible-light-driven CO_2 conversion, Adv. Mater. 35 (2023) 2300643.
[30] C. Zhao, Y. Zhou, D.J. de Ridder, J. Zhai, Y. Wei, H. Deng, Advantages of TiO_2/5A composite catalyst for photocatalytic degradation of antibiotic oxytetracycline in aqueous solution: comparison between TiO_2 and TiO_2/5A composite system, Chem. Eng. J. 248 (2014) 280–289.
[31] D. Pathania, D. Gupta, H. Ala'a, G. Sharma, A. Kumar, M. Naushad, T. Ahamad, S.M. Alshehri, Photocatalytic degradation of highly toxic dyes using chitosan-g-poly (acrylamide)/ZnS in presence of solar irradiation, J. Photochem. Photobiol. Chem. 329 (2016) 61–68.
[32] A. Kumar, A. Kumar, G. Sharma, M. Naushad, F.J. Stadler, A.A. Ghfar, P. Dhiman, R.V. Saini, Sustainable nano-hybrids of magnetic biochar supported g-C_3N_4/$FeVO_4$ for solar powered degradation of noxious pollutants-Synergism of adsorption, photocatalysis & photo-ozonation, J. Clean. Prod. 165 (2017) 431–451.
[33] R. Xu, Y. Peng, Preparation of magnetic g-C_3N_4/Fe_3O_4 composite and its application in the separation of catechol from water, Materials 12 (2019) 2844.
[34] S. Chi, C. Ji, S. Sun, H. Jiang, R. Qu, C. Sun, Magnetically separated meso-g-C_3N_4/Fe_3O_4: bifuctional composites for removal of arsenite by simultaneous visible-light catalysis and adsorption, Ind. Eng. Chem. Res. 55 (2016) 12060–12067.
[35] D. Zhang, S. Cui, J. Yang, Preparation of Ag_2O/g-C_3N_4/Fe_3O_4 composites and the application in the photocatalytic degradation of Rhodamine B under visible light, J. Alloys Compd. 708 (2017) 1141–1149.
[36] X. Zhang, B. Ren, X. Li, Y. Xu, B. Liu, P. Yu, Y. Sun, D. Mei, Efficiently enhanced visible-light photocatalytic activity by in situ deposition of Ag@AgBr on g-C_3N_4/Fe_3O_4 magnetic heterogeneous materials, Separ. Purif. Technol. 254 (2021) 117596.
[37] S. Ghodsi, A. Esrafili, R.R. Kalantary, M. Gholami, H.R. Sobhi, Synthesis and evaluation of the performance of g-C_3N_4/Fe_3O_4/Ag photocatalyst for the efficient removal of diazinon: kinetic studies, J. Photochem. Photobiol. Chem. 389 (2020) 112279.
[38] H.-L. Liu, Y.-R. Chiou, Optimal decolorization efficiency of Reactive Red 239 by UV/TiO_2 photocatalytic process coupled with response surface methodology, Chem. Eng. J. 112 (2005) 173–179.
[39] J. Tang, Y. Liu, Y. Hu, G. Lv, C. Yang, G. Yang, Carbothermal reduction induced Ti3+ self-doped TiO_2/GQD nanohybrids for high-performance visible light photocatalysis, Chem.–Eur. J. 24 (2018) 4390–4398.
[40] M. Berkani, A. Smaali, Y. Kadmi, F. Almomani, Y. Vasseghian, N. Lakhdari, M. Alyane, Photocatalytic degradation of Penicillin G in aqueous solutions: kinetic, degradation pathway, and microbioassays assessment, J. Hazard Mater. 421 (2022) 126719.
[41] G. Moussavi, S. Shekoohiyan, Simultaneous nitrate reduction and acetaminophen oxidation using the continuous-flow chemical-less VUV process as an integrated advanced oxidation and reduction process, J. Hazard Mater. 318 (2016) 329–338.
[42] R. Hao, G. Wang, H. Tang, L. Sun, C. Xu, D. Han, Template-free preparation of macro/mesoporous g-C_3N_4/TiO_2 heterojunction photocatalysts with enhanced visible light photocatalytic activity, Appl. Catal. B Environ. 187 (2016) 47–58.
[43] D. Hernández-Uresti, A. Vázquez, D. Sanchez-Martinez, S. Obregón, Performance of the polymeric g-C_3N_4 photocatalyst through the degradation of pharmaceutical pollutants under UV–vis irradiation, J. Photochem. Photobiol. Chem. 324 (2016) 47–52.
[44] B.K. Gupta, G. Kedawat, Y. Agrawal, P. Kumar, J. Dwivedi, S. Dhawan, A novel strategy to enhance ultraviolet light driven photocatalysis from graphene quantum dots infilled TiO_2 nanotube arrays, RSC Adv. 5 (2015) 10623–10631.
[45] F. Wang, Y. Feng, P. Chen, Y. Wang, Y. Su, Q. Zhang, Y. Zeng, Z. Xie, H. Liu, Y. Liu, Photocatalytic degradation of fluoroquinolone antibiotics using ordered mesoporous g-C_3N_4 under simulated sunlight irradiation: kinetics, mechanism, and antibacterial activity elimination, Appl. Catal. B Environ. 227 (2018) 114–122.
[46] W. Liu, M. Wang, C. Xu, S. Chen, X. Fu, Significantly enhanced visible-light photocatalytic activity of g-C_3N_4 via ZnO modification and the mechanism study, J. Mol. Catal. Chem. 368 (2013) 9–15.
[47] A.K. Ilunga, B.B. Mamba, T.T. Nkambule, Catalytic hydrodehalogenation of halogenated disinfection byproducts for clean drinking water production: a review, J. Water Proc. Eng. 44 (2021) 102402.
[48] B. Kordestani, R.J. Yengejeh, A. Takdastan, A.K. Neisi, A new study on photocatalytic degradation of meropenem and ceftriaxone antibiotics based on sulfate radicals: influential factors, biodegradability, mineralization approach, Microchem. J. 146 (2019) 286–292.
[49] T.J. Al-Musawi, P. Rajiv, N. Mengelizadeh, F.S. Arghavan, D. Balarak, Photocatalytic efficiency of $CuNiFe_2O_4$ nanoparticles loaded on multi-walled carbon nanotubes as a novel photocatalyst for ampicillin degradation, J. Mol. Liq. 337 (2021) 116470.
[50] B. Xie, X. Li, X. Huang, Z. Xu, W. Zhang, B. Pan, Enhanced debromination of 4-bromophenol by the UV/sulfite process: efficiency and mechanism, J. Environ. Sci. 54 (2017) 231–238.
[51] G. Moussavi, M. Rezaei, Exploring the advanced oxidation/reduction processes in the VUV photoreactor for dechlorination and mineralization of trichloroacetic acid: parametric experiments, degradation pathway and bioassessment, Chem. Eng. J. 328 (2017) 331–342.
[52] Y. Jiang, Z. Qin, F. Liang, J. Li, Y. Sun, X. Wang, P. Ma, D.J.J. Song, Vortex-assisted solid-phase extraction based on metal-organic framework/chitosan-functionalized hydrophilic sponge column for determination of triazine herbicides in environmental water by liquid chromatography-tandem mass spectrometry 1638 (2021) 461887.
[53] Q. Xu, L. Zhang, B. Cheng, J. Fan, J. Yu, S-scheme heterojunction photocatalyst, Chem 6 (2020) 1543–1559.
[54] A.A. Al-Ghamdi, R. Jafer, X. Li, P. Zhangc, A new heterojunction in photocatalysis: S-scheme heterojunction, Chin. J. Catal. 42 (2021) 667–669.
[55] F. Beshkar, A. Al-Nayili, O. Amiri, M. Salavati-Niasari, M. Mousavi-Kamazani, Fabrication of S-scheme ZnO/$Zn_3(PO_4)_2$ heterojunction photocatalyst toward photodegradation of tetracycline antibiotic and photocatalytic mechanism insight, Int. J. Hydrogen Energy 47 (2022) 928–939.
[56] H. Yang, A short review on heterojunction photocatalysts: carrier transfer behavior and photocatalytic mechanisms, Mater. Res. Bull. 142 (2021) 111406.
[57] Y. Yang, B. Mao, G. Gong, D. Li, Y. Liu, W. Cao, L. Xing, J. Zeng, W. Shi, S. Yuan, In-situ growth of Zn–$AgIn_5S_8$ quantum dots on g-C3N4 towards 0D/2D heterostructured photocatalysts with enhanced hydrogen production, Int. J. Hydrogen Energy 44 (2019) 15882–15891.
[58] S. Zhang, S. Zhao, S. Huang, B. Hu, M. Wang, Z. Zhang, L. He, M. Du, Photocatalytic degradation of oxytetracycline under visible light by nanohybrids of CoFe alloy nanoparticles and nitrogen-/sulfur-codoped mesoporous carbon, Chem. Eng. J. 420 (2021) 130516.
[59] K. Xu, X. Yang, L. Ruan, S. Qi, J. Liu, K. Liu, S. Pan, G. Feng, Z. Dai, X. Yang, Superior adsorption and photocatalytic degradation capability of mesoporous $LaFeO_3$/g-C_3N_4 for removal of oxytetracycline, Catalysts 10 (2020) 301.
[60] A. Majumdar, U. Ghosh, A. Pal, Novel 2D/2D g-C_3N_4/Bi_4NbO_8Cl nano-composite for enhanced photocatalytic degradation of oxytetracycline under visible LED light irradiation, J. Colloid Interface Sci. 584 (2021) 320–331.
[61] A.I. Vaizoğullar, ZnO/ZrO_2 composites: synthesis characterization and photocatalytic performance in the degradation of oxytetracycline antibiotic, Mater. Technol. 34 (2019) 433–443.
[62] J. Hong, D.K. Hwang, R. Selvaraj, Y. Kim, Facile synthesis of Br-doped g-C_3N_4 nanosheets via one-step exfoliation using ammonium bromide for photodegradation of oxytetracycline antibiotics, J. Ind. Eng. Chem. 79 (2019) 473–481.